On the effects of struts diameter and shape on the European Space Agency deep space antenna directivity and first side lobe

Davide Arenare[1] , Fabio Pelorossi[2], Filippo Concaro[2] and Marco Pasian[1]

[1]Department of Electrical, Computer and Biomedical Engineering, University of Pavia, Pavia, Italy and [2]Directorate of Operations, GSA Section, European Space Operations Centre, European Space Agency, Darmstadt, Germany

Abstract

Large reflector antennas, such as the European Space Agency deep space antennas (DSAs), practically always require struts to support the sub-reflector. While inevitable, they deteriorate the antenna performance. To minimize this deterioration, it is pivotal to understand the role played by different features, including struts diameter and shape. This paper proposes a detailed numerical investigation on the impact of these features on antenna efficiency and side lobes, for a test case comprising both DSA3 and DSA4. It is demonstrated, for the first time in a comprehensive and quantitative way that includes different permutations for the strut design, that both features are significant to define the deterioration, thus providing a significant feedback for struts design.

![CAMBRIDGE UNIVERSITY PRESS]

Introduction

The European Space Agency (ESA) operates, at the present time, a network of three different deep space antennas (DSAs). Namely, DSA1 is located in New Norcia, Australia; DSA2 is located in Cebreros, Spain; DSA3 is located in Malargüe, Argentina. Overall, they are required to operate at several different frequencies (S, X, K, and Ka-band), both for transmitting and receiving. Each antenna is provided with a beam waveguide (BWG) architecture and it exploits a Cassegrain configuration with a 35 m main-reflector and a 4.2 m sub-reflector [1–3]. As can be seen in Fig. 1, the sub-reflector is supported by four metallic struts. These struts are unavoidable, but, due to their position, they interfere with the antenna illumination and, therefore, they have an impact on the antenna performance. Between the variety of effects caused by the presence of the struts we have: a decrease of the antenna efficiency and an increase of parameters such as the side-lobes levels, the cross-polarization, and the antenna noise temperature [4–8]. Over the years, various techniques and approaches were proposed and investigated in order to mitigate such effects [9–12]. When reflectors of this size are considered, numerical analyses are paramount, since the acquisition of systematic measurements is extremely difficult and expensive. Anyway, this kind of simulations, that consider the entire structure of BWG antennas and the struts, are not a common practice, due to the dimension of the elements with respect to the wavelength.

The present paper proposes different simulations on the impact of the struts on the antenna efficiency and the side-lobes levels, as well as a subsequent detailed analysis of the relationship between these parameters and the struts shape and diameter. This allows for deriving important indications, and guidelines, for the design. Such numerical investigations were triggered by the design and construction of a new DSA (DSA4), which is currently under development in Australia, close to DSA1, by a consortium of European companies, European Alliance for Deep Space Antennas, formed by Thales Alenia Space, Schwartz-Hautmont, and Mtex Antenna Technology. An earlier version of this paper was presented at the 52nd European Microwave Conference and was published in its proceedings [13]. More in detail, in paper [13] it was presented a first comparison between the struts of the operational DSA3 and the ones of the upcoming DSA4. This was followed by a second paper [14], in which the authors proposed a preliminary evaluation about the impact of the radius on the straight struts of DSA3. However, a lack of comprehension remained, due to the non-systematic nature of papers [13, 14]. Instead, in this paper, the aim is to provide a better picture about some different aspects concerning the impact on antenna performance of struts, namely strut diameter and shape, leveraging on a more complete set of analyses and simulations, evaluating also virtual intermediate cases that can help to understand the different situations. In particular, six different situations will be considered in the next sections, including the actual DSA3, the forthcoming DSA4 and four in-between

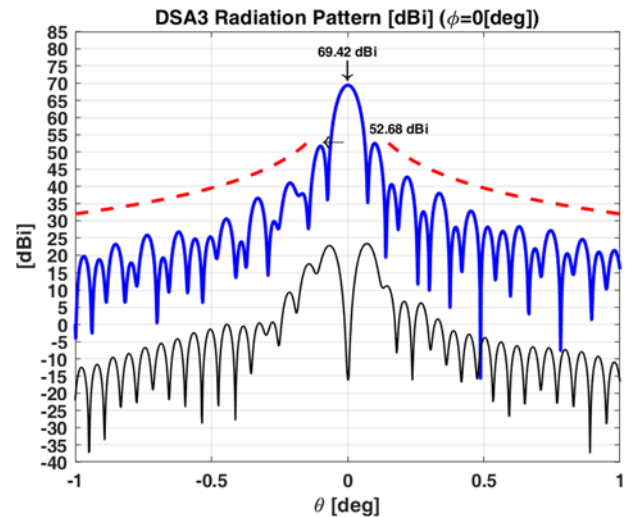**Figure 1.** Photograph of DSA3, Malargüe, Argentina.

Figure 2. Example of DSA3 radiation pattern, co-polar (blue line) and cross-polar (black line) in circular polarization, ITU mask is included (red line). The value of the peak directivity and the first side lobe are reported. Angular cut $\Phi = 0$.

configurations in order to better understand the main novelties among the two DSA struts architectures. All simulations are done in X-band. While this is a choice of opportunity due to the excessive computational time that a simulation at higher frequencies would require, at the same time it also represents probably the most interesting case, as in K- and Ka-band the struts are considerably larger in term of wavelength, thus their impact is expected to be more predictable even without dedicated numerical simulations. Overall, the presented results allow, for the first time in a comprehensive and quantitative way that includes different permutations for the struts design, to understand the significance of the different parameters on the antenna performance.

DSA3

The entire DSA3 structure (entire BWG + double reflector system) is modeled in TICRA GRASP, a commercial tool based on the physical optics (PO), also considering the spherical wave expansion (SWE) file of the real feed implemented in the operational antenna and the shaped geometries of the main- and sub-reflector. Moreover, in order to correctly avoid in the directivity computation, the portion of power that is blocked by the sub-reflector, a hole of the same diameter is inserted in the center of the main-reflector surface. All the different modeled parts are considered as perfect electric conductor (PEC) in GRASP, since in the reality they are fabricated in aluminum, thus, for the purpose of this paper, the difference would be negligible. Once the antenna modeling is completed, the PO simulations are executed at the frequency of 8.45 GHz, which is the central frequency of the receiving X-band (8.40–8.50 GHz). This frequency was chosen for a variety of reasons. From a computational point of view, it is a sensible choice to keep the simulation time within feasible, although still significant limits. On the other hand, DSA3 is currently operating with the same X-band feed that will be exploited for DSA4, this means that the same SWE file can be used in GRASP, removing a degree of freedom from the comparison between the two antennas.

Case without the struts

A first simulation is run without considering the impact of the struts on the antenna performance, that is also the stan-

dard simulation that is done for this kind of projects. An example of the antenna radiation pattern, including the relative International Telecommunication Union (ITU) mask (ITU-Radio and Regulations Appendix Annex III), can be seen in Fig. 2, considering the angular range in θ from -1 to $+1°$. Only one cut over Φ is shown since both the main- and the sub-reflector are rotationally symmetric, thus the minor changes over Φ are not relevant for the scopes of this paper. As reported, the maximum directivity obtained is equal to 69.42 dBi, while the first side-lobe value is -16.74 dB below this peak. From the directivity value, an antenna efficiency equal to 91.09 % can be retrieved.

Case with the struts

Subsequently, the struts are included in the GRASP model, modeled as made out of PEC, like the other antenna components. As it can be seen from the comparison between Figs. 1 and 3, only the inner part of the struts of DSA3 is taken into account. This is done because the inner portion is by far the one with the highest impact on the antenna performance, due to the fact that the simulations in this paper consider the feed as starting point and that thinner and outer part of the struts have an identical diameter. It is worth noting that this choice is also helping to keep the computational time under control. Considering the machine used for the simulations in this paper, equipped with two processors Intel® Xeon® CPU E5-2630 v3 at 2.40 GHz and 128 GB RAM, the computational time including the struts is around 15 days. Anyway, while this choice may have an impact on the specific numbers presented in the paper, it does not affect the trend described and the conclusions drawn.

For DSA3, the inner strut is a straight tube from the main- to the sub-reflector, with a circular cross section featuring a radius of approximately 15 cm and a length exceeding 10 m. This description holds also for the previous DSAs (DSA1 and DSA2).

In general terms, describing the interaction between the struts, the main- and the sub-reflector, three important mechanisms by which the strut scattering influences the antenna radiation can be highlighted, as reported in schemes depicted in Fig. 4. In the first
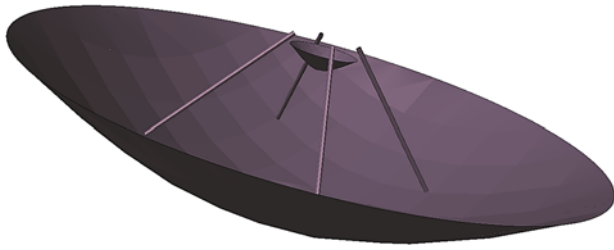
Figure 3. DSA3 GRASP model of main- and sub- reflector with the inner part of the struts.
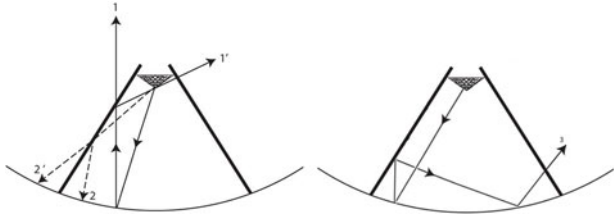

Figure 4. Scheme of interaction between main- and sub-reflector and struts. Illumination directly from the main reflector (lines 1 and 1'), shadowing effect between sub- and main-reflector (lines 2 and 2'), double bouncing effect (line 3). Derived from paper [15].

Figure 5. Example of DSA3 radiation pattern with struts, co-polar (blue line) and cross-polar (black line) in circular polarization. ITU mask is included (red line). The value of the peak directivity and the first side lobe are reported. Angular cut $\Phi = 90°$, struts out of the plane.

Figure 6. Example of DSA3 radiation pattern with struts, co-polar (blue line) and cross-polar (black line) in circular polarization. ITU mask is included (red line). The value of the peak directivity and the first side lobe are reported. Angular cut $\Phi = 135°$, struts in the plane.

place, each strut is illuminated by the field reflected from the main-reflector. Then, we can highlight a shadow-like effect between the sub- and the main-reflector, that as an impact on the illumination of the main-reflector and therefore on its surface currents. In addition, a double bouncing effect between the struts and the underneath portion of the main-reflector can be pointed out ([13] and [14]).

In order to take into account the effects described above, the simulation setup in GRASP has to be specifically modified. More in detail, it is needed both to added new commands to include the struts in the simulation process and to modify already existing commands, for example, in order to correctly compute the currents on the main-reflector surface that now are generated also with the contribution of the struts. This modification rises the computational time in a highly significant way, for this reason it was decided to do not add, on top of standard PO simulations, extra calculations based on the physical theory of diffraction (PTD), normally used to account, with a higher accuracy, for diffraction effects. In particular, in our case, it was evaluated that the potential extra plus given by PTD did not worth the increased computational time. This is because the ratio between the strut diameter and the wavelength, even in X-band, is approx. equal to 10. With this in mind, the significance of PTD results would be largely out weighted by the computational effort required to have PTD results under convergence for such a large antenna.

In Figs. 5 and 6, two cuts of the antenna radiation pattern are shown. As before, the graphs include the ITU mask and a theta range going from −1 to +1°. In this case, two different Φ angles are presented, because the struts break the rotational symmetry of the main- and sub-reflector. In particular, the cut at $\Phi = 90°$, that is not including any strut in its plane, and the cut at $\Phi = 135°$, that it is including struts in its plane, are reported.

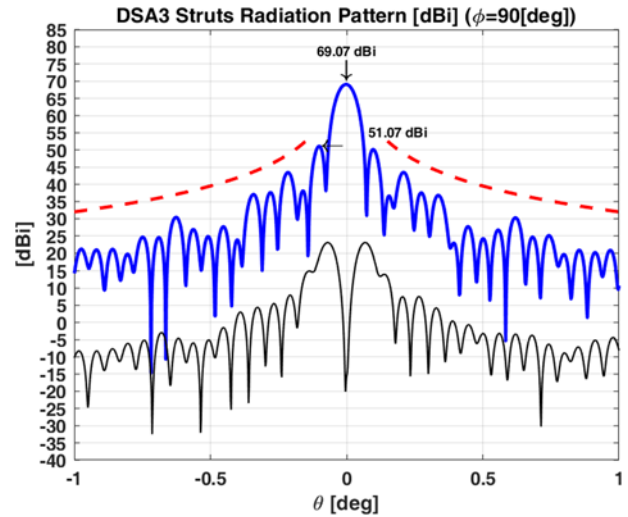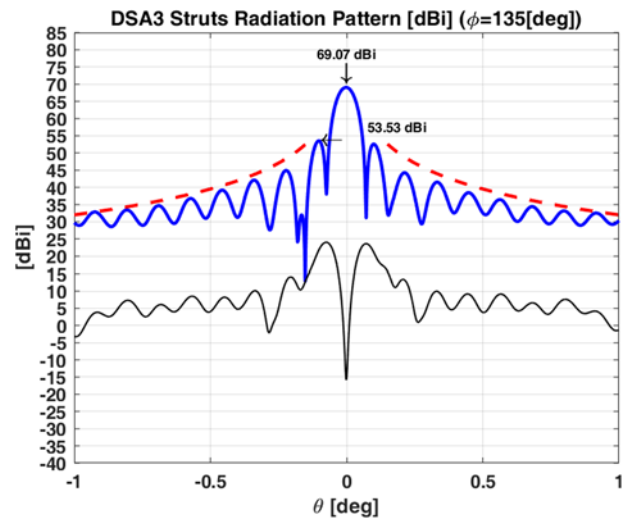It can be noted how relevant is the side-lobes deterioration, especially when the struts belong to the plane considered in the cut. By comparing these results with the ones presented in the previous section, we can derive a drop in the maximum directivity equal to −0.35 dB, from 69.42 dBi down to the value of 69.07 dBi. Regarding the side-lobe level, the max value below this new peak is equal to −15.54 dB. Overall, the new computed efficiency of DSA3 results to be 84.04%, thus the struts efficiency, calculating as the ratio between the antenna efficiencies with and without struts, amounts to 92.26%. This value is important in order to quantify the detrimental impact of the struts on the overall antenna performance.

As anticipated in the introduction, struts can also cause an increase of the cross-polarization component. This effect can be seen easily comparing Figs. 2 and 6. However, for such antennas, in absolute terms the cross-polar component is so low (e.g., 40 dB lower than the co-polar component, calculated within the −3 dB
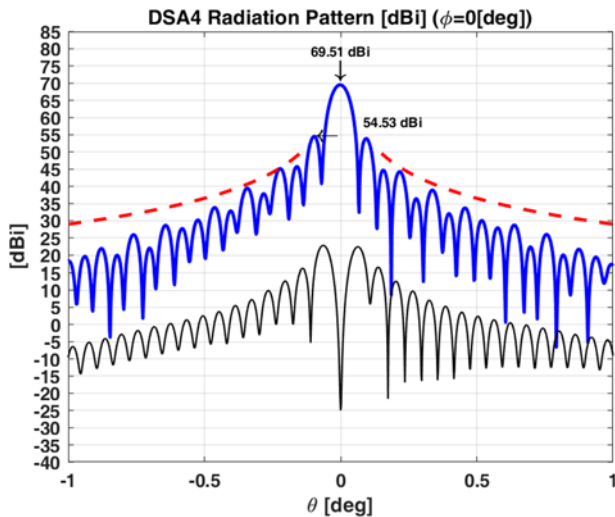
Figure 7. Example of DSA4 radiation pattern, co-polar (blue line) and cross-polar (black line) in circular polarization, ITU mask is included (red line). The value of the peak directivity and the first side lobe are reported. Angular cut $\Phi = 0$.

Figure 8. DSA4 struts, CAD model.

Figure 9. DSA4 GRASP model of main- and sub-reflector, with the inner part of struts.

contour of the main lobe) that those minor variations are hardly of any interest for practical applications, where the relevant fraction of the cross-polar is the one within the co-polar main lobe.

DSA4

The same procedure was exploited to analyze the effects of the struts on the upcoming DSA4. At first, the DSA4 optics and struts, which largely differ from that of DSA3, was modeled in TICRA GRASP, including the shaped surfaces of the reflectors, but still using the SWE file considered before at 8.45 GHz for DSA3.

Case without the struts

As done for DSA3, at beginning the struts are not considered in the simulations. Figure 7 shows an example of the antenna radiation pattern, including the relative ITU mask, which is 3 dB lower with respect to the one considered for DSA3. This is due to the different site region where the upcoming antenna will be located (Australia instead of South America). Once again the θ angular range is between -1 and $+1°$.

The maximum directivity value obtained through the simulations is 69.51 dBi, that results in an efficiency of 93.00%. Considering the side-lobe level, the maximum it is found to be -14.98 dBi below this peak.

Case with the struts

At this point, the struts are added in the simulation environment. As mentioned in the introduction section, the struts of the forth coming DSA4 are going to be different from the ones manufactured for the previous DSAs. The new architecture will still be based on a circular shape, but it will feature two main differences. The radius of the tubes will be smaller than before, approximately 30% less (roughly 11 cm), and a length of 12 m. The second novelty results more visible in Fig. 8, where the CAD model of the structure is reported. In the new structure, each strut will not be a straight tube, but more like four smaller segments that are forged in a bent

architecture. Figure 9 instead represents the struts GRASP model, including, as before, only the inner portion.

In the next graphs (Figs. 10 and 11), two different cuts of the antenna radiation pattern are reported, following the same color scheme of the pattern shown before. Also this time, in order to better represent the antenna performance, one cut that includes struts in its plane and one that does not are illustrated. The peak in directivity decreases, with respect to the case that does not consider the impact of the struts, by -0.21 dB. The worst value of the first side-lobe value is found to be -14.41 dB below this peak. The relative efficiency value is equal to 88.61%. From these numbers we can retrieve the struts efficiency equals to 95.28%, which is higher with respect to the previous struts architecture. It can be observed that the co-polar curve slightly exceeds the ITU mask at certain angles; nevertheless, the result is in line with the specifications defined by ESA according to the ITU principles. The maximum measured exceedance is 1.9 dB with a maximum one allowed of 3 dB. As for DSA3, also in the case of DSA4 can be highlighted a slight increase of the cross-polar component, however the consideration done in the previous paragraph about the minor interest for practical application holds.

The values in Table 1 summarize the configurations of the operational DSA3 and the upcoming DSA4.

In-between configurations

From Table 1, it can be observed that the struts of the upcoming DSA4, thanks to the different design, are going to have a less severe detrimental effect on the antenna radiation. In order to better understand how the two main novelties of the new struts design impact the antenna performance, it was decided to create and simulate four in between configurations of struts architecture. This is done to decouple the effect of the struts radius and of the bent architecture, with the purpose of proving that both these changes are fundamental for the boost in performance given by the DSA4 struts. The aim is to evaluate the impact of these virtual struts from
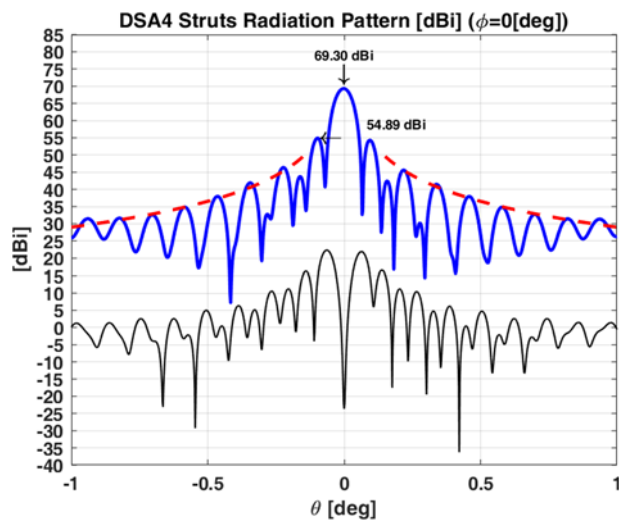
Figure 10. Example of DSA4 radiation pattern with struts, co-polar (blue line) and cross-polar (black line) in circular polarization. ITU mask is included (red line). The value of the peak directivity and the first side lobe are reported. Angular cut $\Phi = 0$, struts in the plane.
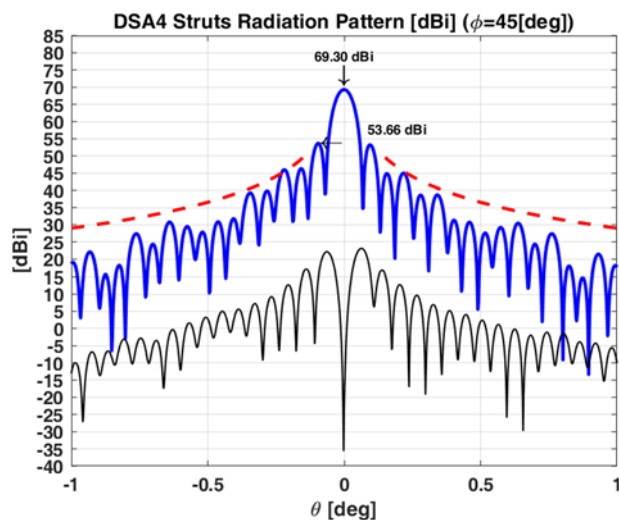

Figure 11. Example of DSA4 radiation pattern with struts, co-polar (blue line) and cross-polar (black line) in circular polarization. ITU mask is included (red line). The value of the peak directivity and the first side lobe are reported. Angular cut $\Phi = 45°$, struts out of the plane.

Table 1. DSA3 and DSA4 summary table

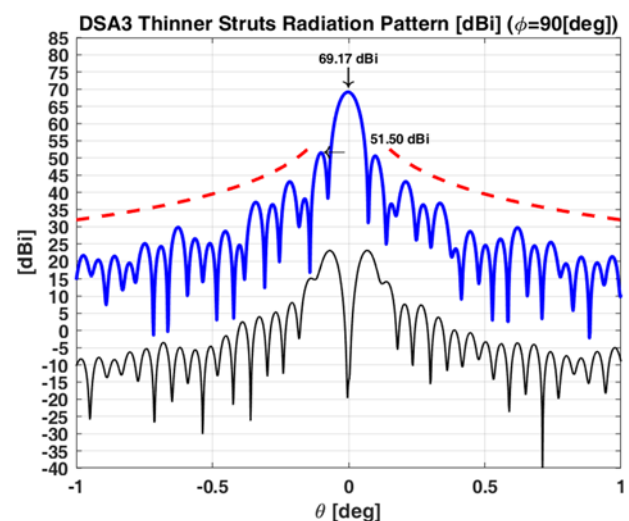| Struts	DSA3		DSA4	
	w/o	ESA DSAs original design for struts	w/o	Latest design for struts
Directivity (dBi)	69.42	69.07	69.51	69.30
1st side lobe (dB)	−16.74	−15.54	−14.98	−14.41
Efficiency (%)	91.09	84.04	93.00	88.61
Struts efficiency (%)	/	92.26	/	95.28

Figure 12. Example of DSA3 with thinner struts radiation pattern, co-polar (blue line) and cross-polar (black line) in circular polarization. ITU mask is included (red line). The value of the peak directivity and the first side lobe are reported. Angular cut $\Phi = 90°$, struts out of the plane.

an electromagnetic point of view, without any consideration about the mechanical one, which is out of scope in this paper, but the main concern when the struts are designed. From a mechanical point of view, with a bent architecture, the gravity load generated by the sub-reflector mass is better supported with respect to straight struts, as much as arches are better structures compared to beams in civil engineering. At the end of the day, this means that smaller-radius struts can be used, minimizing the cost, and obviously the impact on the Electro-Magnetic (EM) performance. In this section, the aim is to evaluate the impact of the struts strictly from an electromagnetic point of view. This is done in order to demonstrate that bended struts are beneficial on their own, and not only because of the smaller diameter, for the antenna performance. This is because the impinging field is scattered in several directions, instead of a

few specific angles as done by straight struts, thus mitigating the possibility of a constructive interference for the scattered field.

Thinner and intermediate DSA3-like struts

As first middle configuration, it was decided to exploit the DSA3 GRASP model, modifying the struts radius, in order to meet the radius of the ones of DSA4, but keeping the straight tubes architecture. In Figs. 12 and 13, two cuts are shown to describe the antenna radiation pattern. The cut at $\Phi = 90°$ and the cut at $\Phi = 135°$, which is the one including struts in its plane, are shown. The peak in directivity changes from 69.07 dBi of the operational DSA3, to 69.17 dBi in this virtual configuration. Therefore, the antenna efficiency increases by almost 2% (from 84.04% to 86.00%). Regarding the side-lobes level, the worst value is located −15.86 dB below the apex in directivity. The struts efficiency can be calculated equal to 94.41%, higher than DSA3, but lower than DSA4. Another test was done with the same configuration but with a different radius, selected in between the radius of the struts of the operational DSA3 and the one of the upcoming DSA4. In this way it is possible to have a better understanding of how the different parameters vary
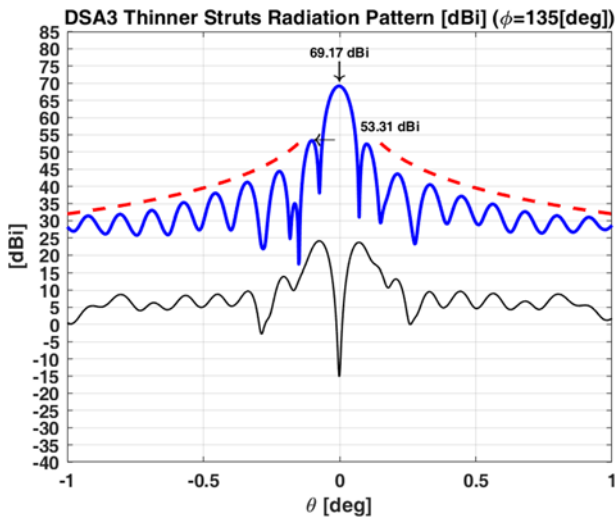
Figure 13. Example of DSA3 with thinner struts radiation patter, co-polar (blue line) and cross-polar (black line) in circular polarization. ITU mask is included (red line). The value of the peak directivity and the first side lobe are reported. Angular cut $\Phi = 135°$, struts in the plane.

Figure 15. Example of DSA3 with thinner struts radiation pattern, co-polar (blue line) and cross-polar (black line) in circular polarization. ITU mask is included (red line). The value of the peak directivity and the first side lobe are reported. Angular cut $\Phi = 135°$, struts in the plane.

Figure 14. Example of DSA3 with intermediate struts radiation patter, co-polar (blue line) and cross-polar (black line) in circular polarization. ITU mask is included (red line). The value of the peak directivity and the first side lobe are reported. Angular cut $\Phi = 90°$, struts out of the plane.
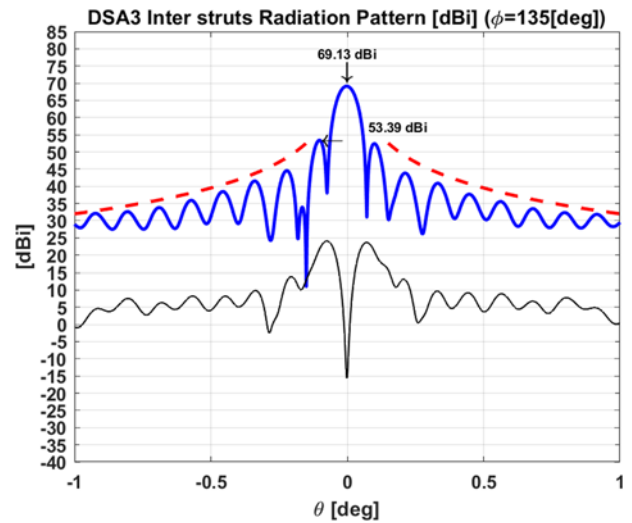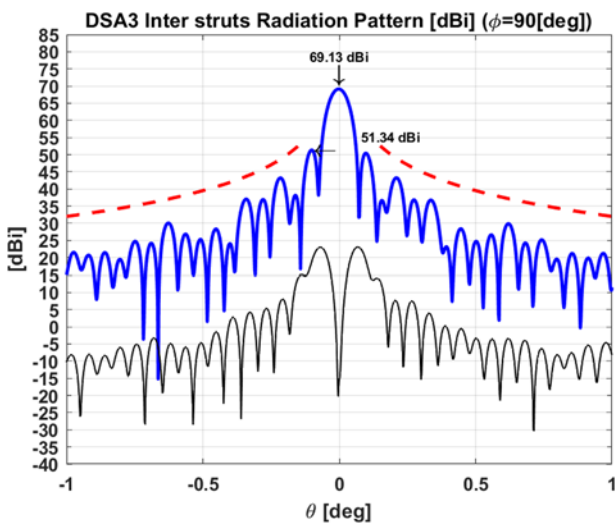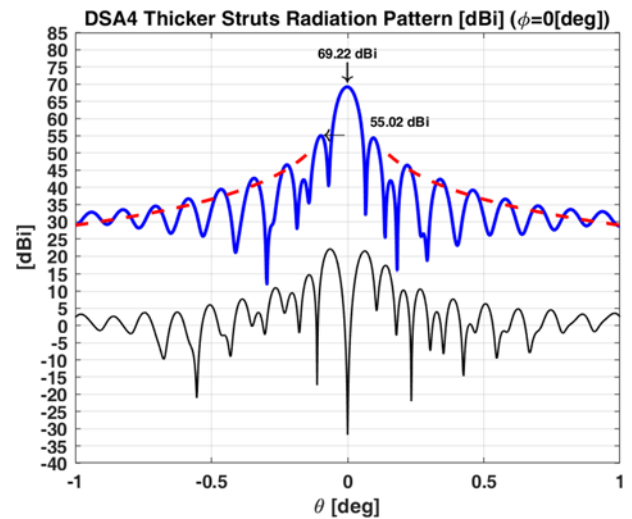

Figure 16. Example of DSA4 with thicker struts radiation pattern, co-polar (blue line) and cross-polar (black line) in circular polarization. ITU mask is included (red line). The value of the peak directivity and the first side lobe are reported. Angular cut $\Phi = 0$, struts in the plane.

according to the radius. In this case, as can be seen in Figs. 14 and 15, the peak in directivity is 69.13 dBi, which corresponds to an antenna efficiency of 85.21%, with a resulting struts efficiency of 93.54%. The worst side-lobe level is at −15.74 dB.

Thicker and intermediate DSA4-like struts

Another tested configuration exploits instead the DSA4 GRASP model. In this case, the bent architecture is maintained, while the diameter of the tubes is increased in order to meet the one of the DSA3 struts, approximately 30 cm. The two cuts describing the antenna radiation pattern are reported. In Fig. 16 is depicted the cut at $\Phi = 0$, which is the one including struts in its plane, and in Fig. 17 is depicted the cut at $\Phi = 135°$.

The peak in directivity corresponds to 69.22 dBi, versus 69.30 dBi of the upcoming DSA4. This means that the antenna efficiency drops from 88.61% down to 86.99%. If we look at the side lobes, the worst first side-lobe level is found −14.02 dB below the peak. It can also be noted that the side lobes are also borderline considering the ITU mask. From these numbers it possible to compute a struts efficiency of 93.54%, again an in between result if we consider the operational DSA3 and the actual model of the forthcoming DSA4. As done for the DSA3 like configuration, also in this paragraph is selected the same radius in between the one of the struts of the operational DSA3 and the one of the upcoming DSA4. In this case, as can be seen in Figs. 18 and 19, the peak in directivity is 69.28 dBi, which corresponds to an antenna efficiency of 88.20%, with a resulting struts efficiency of 94.84%. The worst side-lobe level is at −14.35 dB.
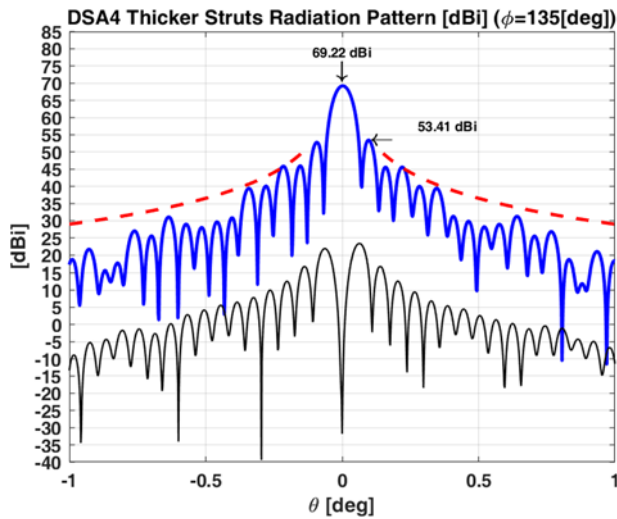
Figure 17. Example of DSA3 with thicker struts radiation pattern, co-polar (blue line) and cross-polar (black line) in circular polarization. ITU mask is included (red line). The value of the peak directivity and the first side lobe are reported. Angular cut $\Phi = 135°$, struts off the plane.

Figure 19. Example of DSA3 with thicker struts radiation pattern, co-polar (blue line) and cross-polar (black line) in circular polarization. ITU mask is included (red line). The value of the peak directivity and the first side lobe are reported. Angular cut $\Phi = 135°$, struts off the plane.
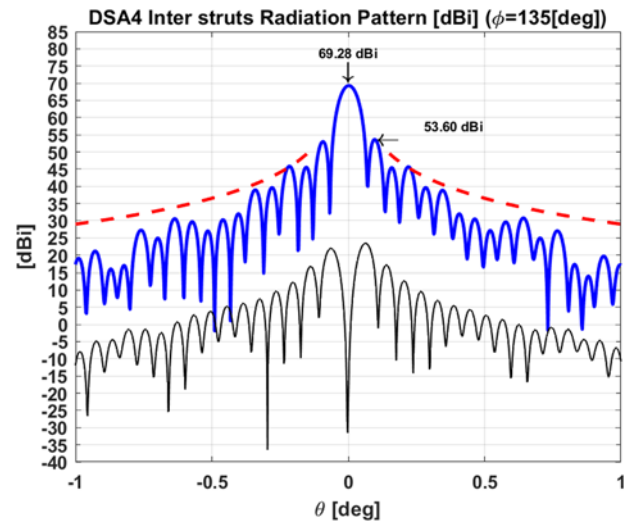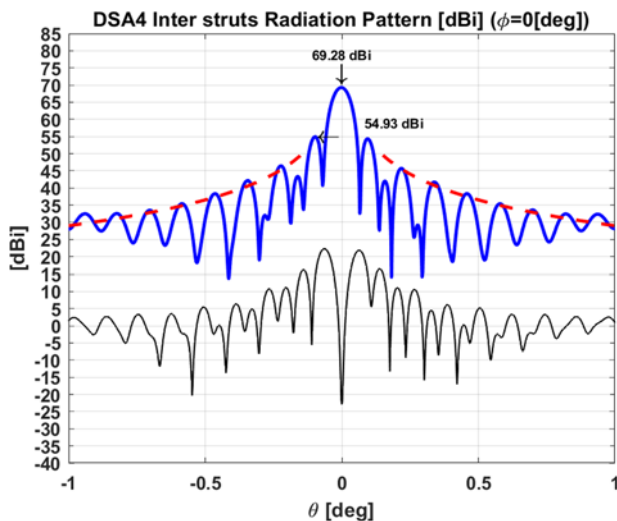

Figure 18. Example of DSA4 with thicker struts radiation pattern, co-polar (blue line) and cross-polar (black line) in circular polarization. ITU mask is included (red line). The value of the peak directivity and the first side lobe are reported. Angular cut $\Phi = 0$, struts in the plane.

In Table 2 instead can be found a comparison between the performance variations caused by the different struts design considering also the virtual in-between configurations.

Currents on struts

Another analysis that was carried out was to investigate the currents generated on the surface of the struts by the main- and sub-reflector. Also in this case GRASP was used, exciting the model from the feed, as outlined in section "Case with the struts," both for DSA3 and DSA4. The results, showing only the face of the struts oriented toward the hole in the main reflector, are depicted in Figs. 20 and 21. In particular, the magnitude of the surface current was calculated on the cylindrical surface of the
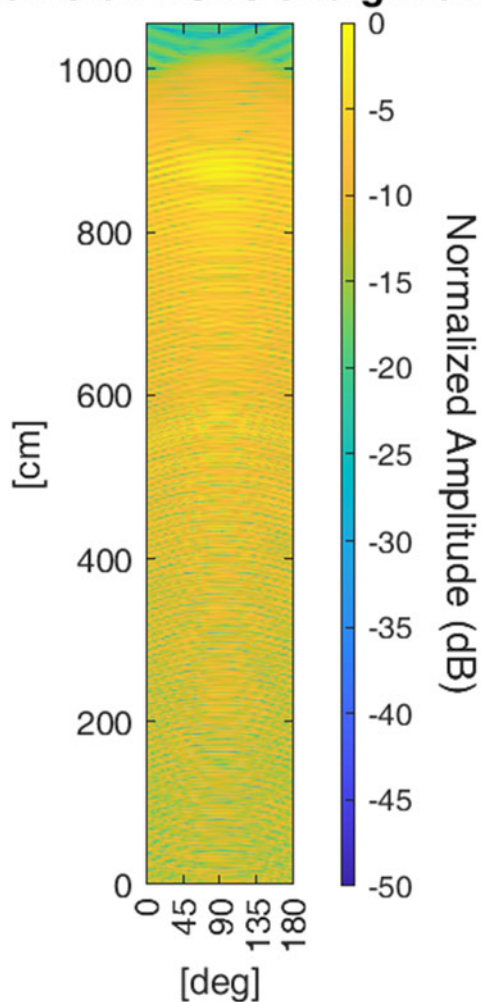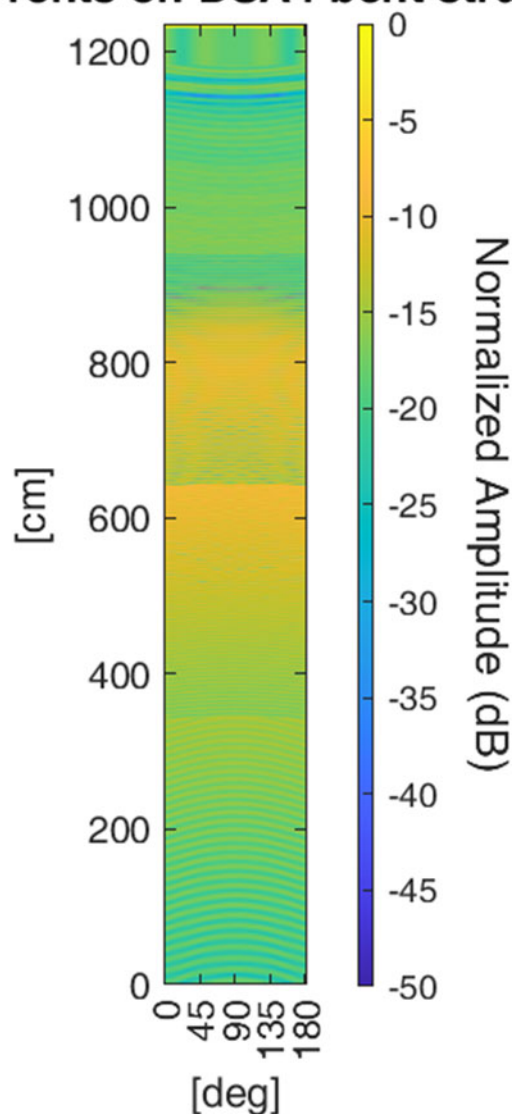
strut, and this cylindrical surface is made planar, in the graphs above, to ease the representation. More in detail, the horizontal axis reports the angular rotation along the axis of the cylindrical strut (being the coordinate at 90° the direction looking toward the center of the antenna), while the vertical axis reports the vertical displacement from the starting tip (0 cm, at the main reflector surface) to the end tip (more than 1000 cm and 1200 cm for DSA3 and DSA4, respectively, at the sub reflector surface) of the strut.

For DSA3, it can be appreciated a relatively uniform distribution of the amplitude of the surface current. This is due to the diameter of the struts, approx. 10 times larger than the wavelength, which let the field, hence the current, envelope the struts rather uniformly from 0 to 180°. In addition, the amplitude of the current is pretty much uniform from 0 cm up to approx. 1000 cm because the inclination of the strut, approx. 47°, with respect to the propagation of the field is constant. Finally, the weak amplitude above 1000 cm is due to the fact that the end tip of the strut is partially masked by the sub-reflector.

For DSA4, first of all, it can be appreciated a slight transition, in the graph, between the four different sections of strut. This is due to the fact the four different sections are at different angles with respect to each other, and this naturally creates a discontinuity. Also in this case, it can be appreciated a relatively uniform distribution of the amplitude of the surface current for what concerns the angular variable. Again, this is due to the ratio between the diameter of the strut and the wavelength, approx. equal to 7, which let the field, hence the current, envelope the struts rather uniformly from 0 to 180°. Instead, the amplitude of the surface current is not uniform moving from 0 cm up to approx. 1200 cm. In particular, at the beginning and at the end of the strut it is weaker. This is due to the fact that the inclination of the strut for the first section is almost vertical (approx. 10°), while the inclination of the strut for the fourth section approaches the horizontal plane (approx. 65°). At those inclinations, the projection of the polarization components of the field parallel to the strut is weaker.

Table 2. Comparison table of all configurations

Configuration	DSA3 and DSA4 performance variation with respect to their respective "no-struts" case					
	DSA3 ESA DSAs original design for struts (original diameter, straight)	DSA3 Interm. struts (interm. diameter, straight)	DSA3 Thinner struts (thinner diameter, straight)	DSA4 Thicker struts (thicker diameter, bent)	DSA4 Interm. struts (interm. diameter, bent)	DSA4 Latest design for struts (thinner diameter, bent)
Directivity (dB)	−0.35	−0.29	−0.25	−0.29	−0.23	−0.21
1st side lobe (dB)	+1.2	+1	+0.88	+0.78	+0.63	+0.57
Efficiency (%)	−7.05	−5.87	−5.09	−6.01	−4.80	−4.39

Figure 20. Currents on a DSA3 straight strut.

Figure 21. Currents on a DSA4 bent strut.

Conclusions

This paper presented the results of numerical simulations regarding the impact of the struts architecture on the antenna efficiency and side lobes, for the first time in a comprehensive way that includes different permutations for the struts design, which allows to quantify how the struts design affects the antenna performance.

A comparison between the operational DSA3 and the upcoming DSA4, considering both the ideal configuration, without the struts, and the real one was reported. The new DSA4 struts will indeed

exploit a different design (thinner radius and bent architecture) with respect to the previous DSAs, with the aim of having a less severe impact on the antenna performance. The described results are in line with this goal. The following step was to decouple the effects of the two main novelties of the DSA4 struts architecture by modeling four in-between DSA configurations, one implementing a thinner version of the DSA3 straight tubes struts and another one implementing a thicker version of the DSA4 bent architecture struts, as well as two additional intermediate cases in order to highlight the trend of the struts impact varying the radius of the different structures. The results obtained were in both cases an improvement of the operational DSA3 in terms of directivity, thus efficiency, and side lobes, but at the same time they did not match the outcome achieved with the DSA4 design. Indeed, it appears that the struts diameter, as expected, significantly affects the antenna radiation. However, it is also evident that also the bent architecture is playing a role that is not negligible in defining the overall antenna performance, at a cost of an increased complexity for the mechanical design and antenna installation.

References

1. **Vassallo E, Martin R, Madde R, Lanucara M, Besso P, Droll P, Galtie G and De Vicente J** (2007) The European Space Agency's deep-space antennas. *Proceedings of the IEEE* **95**(11), 2111–2131.
2. **Bozzi M, Cametti M, Fornaroli M, Maguire P, Marti S, Pasian M, Perregrini L and Rawson S** (2012) Future architectures for European Space Agency deep space ground stations. *IEEE Antennas and Propagation Magazine* **54**(1), 254–263.
3. **Pasian M, Cametti M, Bozzi M and Perregrini L** (2013) Multiphysics design and experimental verification of a quad-band dichroic mirror for deep space ground stations. *IET Microwaves, Antennas and Propagation* **7**(6), 391–398.
4. **Ruze J** (1968) Feed support blockage loss in parabolic antennas. *Microwave Journal International Edition* **11**, 76–80.
5. **Ko WL, Mittra R and Lee SW** (1984) Aperture blockage in reflector antennas. *IEEE Antennas and Propagation Magazine* **32**(3), 282–287.
6. **Landecker TL, Anderson MD, Routledge D, Smegal RJ, Trikha P and Vaneldik JF** (1991) Ground radiation scattered from feed support struts: A significant source of noise in paraboloidal antennas. *Radio Science* **26**(2), 363–373.
7. **Cheng J and Mangum JG** (1998) Feed leg blockage and ground radiation pickup for Cassegrain antennas. *MMA Memo 197*.
8. **Ravanelli R, Lubrano V and Iannicelli C** (2012) Struts scattering effects on high performance spacecraft antenna. In *6th European Conference on Antennas and Propagation (EUCAP)*, Prague, Czech Republic, 26–30 March 2012.
9. **Satoh T, Endo S, Matsunaka N, Betsudan S, Katagi T and Ebisui T** (1984) Sidelobe level reduction by improvement of strut shape. *IEEE Antennas and Propagation Magazine* **32**(7), 698–705.
10. **Kildal P-S, Olsen E and Anders Aas J** (1988) Losses, sidelobes, and cross polarization caused by feed-support struts in reflector antennas: Design curves. *IEEE Antennas and Propagation Magazine* **36**(2), 182–190.
11. **Jacobsson P and Rylander T** (2009) Shape optimization of the total scattering cross section for cylindrical scatterers. *Radio Science* **44**(4), 1–14.
12. **Riel M, Brand Y, Demers Y and De Maagt P** (2012) Performance improvements of center-fed reflector antennas using low scattering struts. *IEEE Antennas and Propagation Magazine* **60**(3), 1269–1280.
13. **Arenare D, Pelorossi F, Concaro F and Pasian M** (2022) Numerical investigation about the impact of struts on the European Space Agency Deep Space Antennas efficiency and sidelobes. In *2022 52nd European Microwave Conference (EuMC)*, Milan, Italy, 856–859.
14. **Arenare D, Pelorossi F and Pasian M** (2023) Impact of strut diameter on the European Space Agency Deep Space Antennas efficiency and sidelobes. In *2023 European Conference on Antennas and Propagation (EuCAP)*, Florence, Italy.
15. **Pontoppidan K** (2005) GRASP9 technical description. TICRA, February.

Davide Arenare (graduate student member, IEEE) was born in 1996. He received the master's degree (cum laude) in Electronic Engineering from the University of Pavia, Pavia, Italy, in 2020, with a thesis developed in collaboration of the European Space Agency in the context of a traineeship program. Currently, he is pursuing the Ph.D. degree with the Microwave Laboratory (University of Pavia), working on the analysis and design of next-generation ground stations and, in particular, on the NNO-3 project. In the framework of this project, in 2023, he spent 3 months at Thales Alenia Space Toulouse as a partner in situ.

Fabio Pelorossi received a B.Sc. in Electronic Engineering in 2008, an M.Sc. with specialization in Telecommunication Systems in 2011, and a Ph.D. in Electromagnetics in 2016 from the Sapienza University of Rome, Rome, Italy. In 2011, he was a Trainee at the European Space Research and Technology Centre (ESTEC), European Space Agency (ESA) in The Netherlands, working on advanced antenna payload configurations. Since December 2011, he has been working as Antenna Engineer in the ground systems division at the European Space Operations Centre (ESOC), Darmstadt, Germany. His main area of expertise lies in the antenna front-end design and validation. He is responsible, in the role of technical officer, of several ESA technology studies and in operational activities for the support of ESA launches, earth observation, and deep space missions.

Filippo Concaro graduated in Electronic Engineering from the University of Pavia, Italy, in 2003. Since then, he worked in the European Space Operations Centre (ESOC) and EUMETSAT in Ground Station Engineering. He was involved in the design and testing of several Ground Station projects all over the European Space Agency Tracking Network (ESTRACK). In particular, he was responsible for the XAA (X-Band Acquisition Aid), NNO-2, MAL-X, and SNOWBEAR antenna projects and the cryo feeds installations in the European Space Agency deep space antennas. He is currently the RF responsible for the NNO-3 deep space antenna project.

Marco Pasian was born in 1980. He received the M.Sc. degree (cum laude) in Electronic Engineering and the Ph.D. degree in Electronics and Computer Science from the University of Pavia, Pavia, Italy, in 2005 and 2009, respectively. From 2004 to 2008, he spent periods at the European Space Agency, Darmstadt, Germany; the Carlo Gavazzi Space, Milan, Italy; and the TNO, Defense, Security and Safety, The Hague, The Netherlands. From 2009 to 2013, he was Postdoctoral Researcher with the Microwave Laboratory, University of Pavia, where he was Assistant Professor from 2013 to 2020 and has been Associate Professor since 2020. He has been Principal Investigator, or Unit Coordinator, for several competitive European and Italian grants. In addition, he has also been Project Manager, Scientific Manager, and Consultant for several projects in collaborations with European and Italian research centers and industries, including the European Space Agency. His research interests include microwave- and millimeter-wave components, systems, and technologies, including substrate integrated waveguides, for space applications and investigation of complex, nonstandard media, most notably for biomedical imaging and cryosphere monitoring. Prof. Pasian is member of the European Microwave Association (EuMA), senior member of the Institute of Electrical and Electronics Engineers (IEEE), and member of the Italian Society on Electromagnetism (SIEm). He was the Technical Program Committee (TPC) Chair at the European Microwave Conference 2022, and served as TPC Co-Chair, TPC member, Conference Prize Committee Chair, and Finance Chair for other EuMA and IEEE conferences. He is Editor-in-Chief of the EuMA's *International Journal of Microwave and Wireless Technologies* and Associate Editor of the *IEEE Journal of Electromagnetics, RF and Microwaves in Medicine and Biology*.